Ground Movement Predictions for Braced Excavations in Undrained Clay

Ashraf S. Osman[1] and Malcolm D. Bolton[2]

Abstract: The writers introduce a design approach for braced excavations based directly on the data of carefully chosen soil tests, conceived within the framework of plasticity theory, but allowing for strain hardening. Mobilized shear stresses beneath and around braced excavations are found by a stability calculation based on a proposed plastic deformation mechanism. Strains required to mobilize these stresses are deduced from a direct simple shear test on a representative sample taken from a selected location in the plastic zone of influence. These strains are entered into a simple plastic deformation mechanism to predict boundary displacements. Hence, the proposed Mobilizable Strength Design (MSD) method can satisfy both safety and serviceability in a single step of calculation, without the need for finite element analyses. In this method, design parameters can be chosen rationally with regard to the initial state of soil, the stiffness following the appropriate stress path, and the level of acceptable deformations under working conditions. Examples demonstrating the success of the MSD method are given for a variety wall and soil conditions. Comparisons are made both with previously published field studies and with comprehensive nonlinear finite element analyses.

DOI: 10.1061/(ASCE)1090-0241(2006)132:4(465)

CE Database subject headings: Excavation; Clays; Plasticity; Displacement.

Introduction

During recent decades, there has been an increasing use of retaining walls for basements and underground roads, for example. The need for construction of excavations in urban areas requires control of the surrounding ground since excessive ground movements damage adjacent properties. Excessive ground movements can also affect the functionality of structures in terms of their appearance, efficiency and durability. Deformation control is often as critical as assurance against collapse (Garrett and Barnes 1984; Raison 1985; Ikuta et al. 1994; Young and Ho 1994; Ou et al. 2000). Therefore, limiting values of displacements or strains should be specified to define serviceability in terms of just-acceptable conditions. Unnecessarily severe restrictions may lead to uneconomic design. Therefore, an accurate prediction of displacements under working conditions is required.

There are two common techniques for estimating wall deflections and soil settlements involving either interpolation from a published empirical database or numerical analysis using finite elements. Soil is quite a complicated material that always shows a nonlinear and sometimes brittle response. Although many aspects of nonlinear soil stiffness are well understood and have been incorporated into numerical models, many of these models are relatively complex and the parameters lack clear physical meaning. Also, these analyses require special soil testing and lengthy computer calculations and therefore occupy a disproportionate time for practicing engineers. This may explain why engineers generally prefer to use design charts which incorporate nondimensional soil strength and stiffness ratios based on rather simple characterizations (Mana and Clough 1981; Clough et al. 1989).

The purpose of this paper is to suggest a new approach to the estimation of ground movement that can incorporate the actual stress-strain data, and the undrained shear strength profile, of the soil on site. At the same time, it is desired to offer the geotechnical engineer a practical design tool. The new approach to the design of braced excavations, set out below, makes clear assumptions about stress equilibrium and strain compatibility through the use of a plastic deformation mechanism. Soil behavior is represented by a direct simple shear (DSS) test curve of mobilized stress and strain. Nonlinear stiffness is therefore accounted for directly—there is no need for constitutive laws or parameters. In this respect, the new approach can be considered an extension of the Massachusetts Institute of Technology (MIT) stress-path method (Lambe 1967).

Plastic Deformation Mechanism

Displacement Field

Following O'Rourke (1993), the incremental lateral displacement profile of a multipropped retaining wall in soft clay subject to excavation beneath the lowest level of support (Fig. 1) can be assumed to conform to a cosine function as follows:

[1]Research Associate, Schofield Centre, Dept. of Engineering, Univ. of Cambridge, High Cross, Madingley Rd., Cambridge CB3 0EL, U.K. E-mail: aseko2@cam.ac.uk

[2]Professor of Soil Mechanics and Director of the Schofield Centre, Dept. of Engineering, Univ. of Cambridge, High Cross, Madingley Rd., Cambridge CB3 0EL, U.K. E-mail: mdb@eng.cam.ac.uk

Note. Discussion open until September 1, 2006. Separate discussions must be submitted for individual papers. To extend the closing date by one month, a written request must be filed with the ASCE Managing Editor. The manuscript for this paper was submitted for review and possible publication on May 27, 2004; approved on July 12, 2005. This paper is part of the ***Journal of Geotechnical and Geoenvironmental Engineering***, Vol. 132, No. 4, April 1, 2006. ©ASCE, ISSN 1090-0241/2006/4-465–477/$25.00.

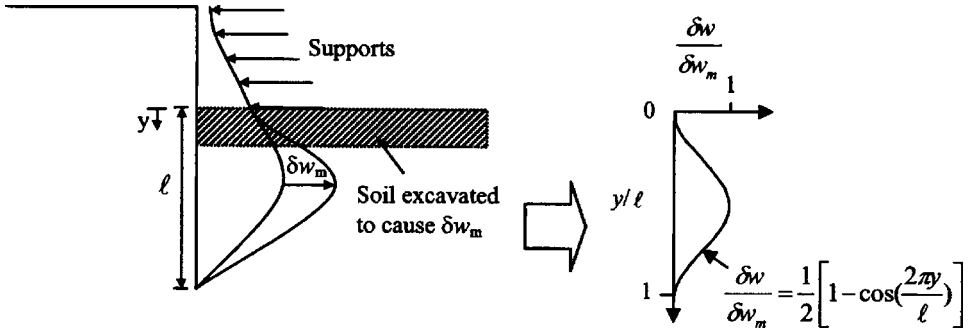

Fig. 1. Incremental displacements in braced excavations [adapted from O'Rourke (1993)]

$$\delta w = \frac{\delta w_m}{2}\left[1 - \cos\left(\frac{2\pi y}{\ell}\right)\right] \tag{1}$$

where δw=incremental wall displacement at any distance y from the lowest wall support; δw_m=maximum incremental displacement; and ℓ=full wavelength of the deformation pattern. Fig. 2 shows that the postulated cosine function conforms generally to the incremental displacements measured on site.

Fig. 3 shows plastic deformation mechanisms proposed by the writers for a multipropped wall supporting an excavation in clay, associated with the incremental lateral displacement generated by excavation of the soil beneath the lowest level of support. In these mechanisms, the wall is assumed to be fixed incrementally in position and rotation at the lowest level of props, which implies that the wall has sufficient strength to avoid the formation of a plastic hinge. The wall and soil are deforming compatibly and the soil deformation follows the cosine function of Eq. (1). The dotted lines with the arrows, in Fig. 3, show the direction of the plastic flow. Along each of these lines the displacement is constant and is given by the cosine function of Eq. (1). Outside the deformation zones, the soil is taken to be rigid. Inside the plastic mechanism, the soil is taken to deform continuously with no slip surfaces. This contrasts with conventional plasticity solutions for the stability of braced excavations (Terzaghi 1943; Bjerrum and Eide 1956; Eide et al. 1972), in which the soil is permitted relative displacements between sliding blocks, and the wall is assumed to be rigid.

The dimensions of the proposed mechanism depend on the wavelength ℓ. The relation between the wavelength and the length s of the wall beneath the lowest support depends on the wall end-fixity condition.

$$\ell = \alpha s \tag{2}$$

where the wall is embedded into a stiff layer beneath the soft clay, such that the wall tip is fully fixed, the wavelength is equal to the wall length (α=1). For short walls embedded in deep very soft clay, the maximum wall deformation occurs at the tip of the wall (Hashash and Whittle 1996) so that the wavelength can be taken to be twice the projecting wall length (α=2). It is common that a wall is embedded in soft or medium stiffness soil where its end is not fixed and the maximum displacement occurs below the excavation level (Clough and Reed 1984; Tanaka 1994). These intermediate cases can be described as restrained-end walls ($1<\alpha<2$).

Distributed Shear Strains

Since there are no slip displacements involved, the deformation in Fig. 3 can be characterized as distributed shearing, with engineering shear strain increments $\delta\gamma$ given by

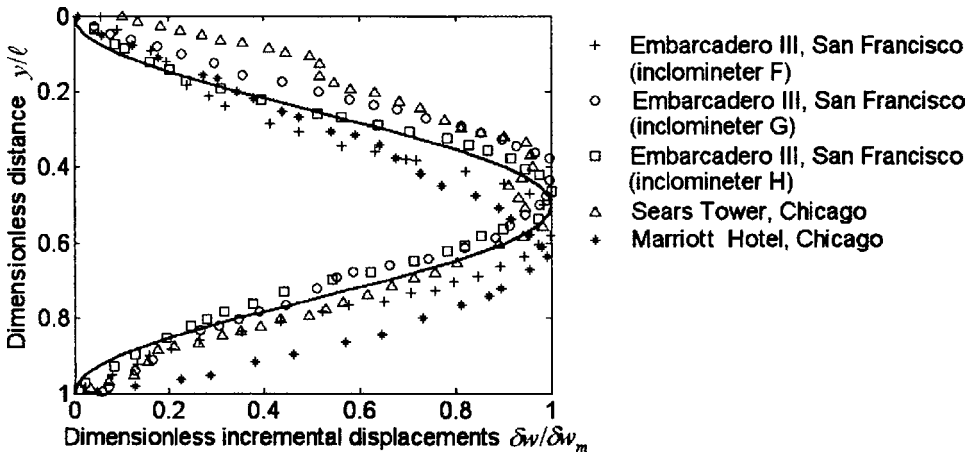

Fig. 2. Comparison of incremental displacement profiles between field inclinometer data and the cosine function [data adapted from O'Rourke (1993); with permission from the Institution of Civil Engineers]

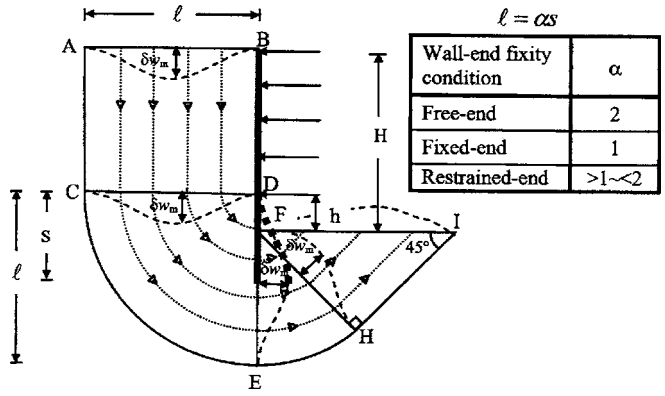

Fig. 3. Plastic deformation mechanisms for braced excavations in clay

$$\delta\gamma = |\delta\varepsilon_1 - \delta\varepsilon_3| = |\delta\varepsilon_1 - (-\delta\varepsilon_1)| = 2|\delta\varepsilon_1| \tag{3}$$

where $\delta\varepsilon_1$ and $\delta\varepsilon_3$=major and minor principal strain increments, respectively. Since the spatial scale is fixed by distance ℓ, all strain components are proportional to $\delta w_m/\ell$. Table 1 defines the engineering shear strain increments in each zone of the proposed mechanism compatible with the incremental wall displacement δw_m. The average shear strain increment $\delta\gamma_{\text{mob}}$ mobilized in the deforming soil due to the incremental wall displacement δw_m can be calculated from the spatial average of the shear strain increments in the whole volume of the deformation mechanism:

Table 1. Shear Strain Increments in the Proposed Deformation Mechanism of Fig. 3.

Zone	Engineering shear strain increment $\delta\gamma$
ABDC	$\left\lvert -\delta w_m \frac{\pi}{\ell}\sin\left(\frac{2\pi x}{\ell}\right)\right\rvert$ x=distance from the wall
CDE	$\left\lvert -\delta w_m \frac{\pi}{\ell}\sin\left(\frac{2\pi r}{\ell}\right) + \frac{\delta w_m}{2r}1-\cos\left(\frac{2\pi r}{\ell}\right)\right)$ r=radial distance from the center of the circular arc (D)
EFH	$\left\lvert -\delta w_m \frac{\pi}{\ell}\sin\left(\frac{2\pi(h+r)}{\ell}\right) + \frac{\delta w_m}{2r} \times\left(\left(1-\cos\left(\frac{2\pi(h+r)}{\ell}\right)\right)\right)\right\rvert$ r=radial distance from the center of the circular arc (F); and h=distance between the lowest support and the excavation level
FIH	$\left\lvert -\delta w_m \frac{\pi}{\ell}\sin\left(\frac{2\pi(h+r)}{\ell}\right)\right\rvert$ r=distance along FH between point F and the intersection with a plastic flow line

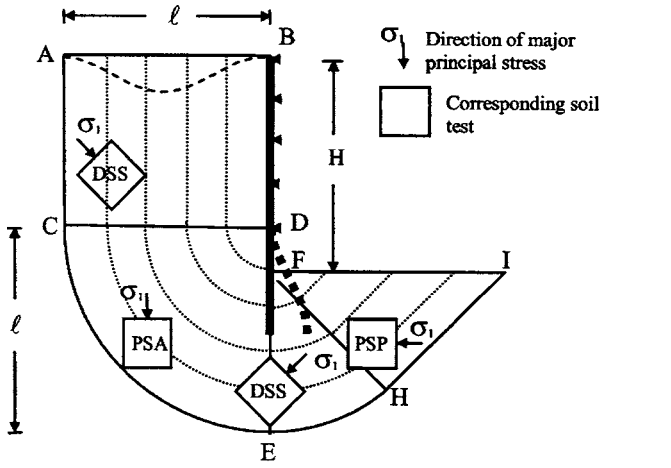

Fig. 4. Direction of major principal stresses consistent with the plastic deformation mechanism

$$\delta\gamma_{\text{mob}} = \frac{\int_{\text{vol}} \delta\gamma d\text{vol}}{\int_{\text{vol}} d\text{vol}} \approx 2\frac{\delta w_m}{\ell} \tag{4}$$

The actual value of $\delta\gamma_{\text{mob}}/(\delta w_m/\ell)$ in any stage of excavation depends somewhat on the current geometry of the mechanism, but it does not deviate from 2.0 by more than 10%. The key importance of Eq. (4) is that it links the average strain increment mobilized in the soil with the maximum incremental displacement of the wall, during any stage of excavation.

Equilibrium

The equilibrium condition of the assumed mechanism, stage by stage, needs to recognize both the profile of undrained strength with depth and the degree to which that strength is mobilized.

In soft clay, the undrained strength generally varies with depth (heterogeneity), and with orientation of the shearing direction (anisotropy). The strength c_{mob} mobilized at any location for any excavation height can be expressed using a factor β on the appropriate undrained strength c_u profile. It is well established that the anisotropy of soft clay can be a significant determinant of excavation stability. For example, Clough and Hansen (1981) show an empirical correction factor based on the observation that triaxial extension tests can give half the undrained strength in triaxial compression, with simple shear roughly halfway between. Fig. 4 shows the orientation of the major principal stress direction within the various zones of shearing in the assumed plastic mechanism, and indicates with a code the soil test configuration that would correctly measure the undrained strength at the specified orientation. In locations marked DSS, the assumed directions of shearing are vertical or horizontal, so the ideal test on a vertical core is a DSS test. In locations marked plane strain active (PSA) and plane strain passive (PSP) the shearing takes place at 45° to the horizontal, and the ideal tests are PSA and PSP, respectively. Since $c_{u,\text{DSS}}$ is roughly the average of $c_{u,\text{PSA}}$ and $c_{u,\text{PSP}}$, and the influence of the PSA and PSP zones in Fig. 4 is

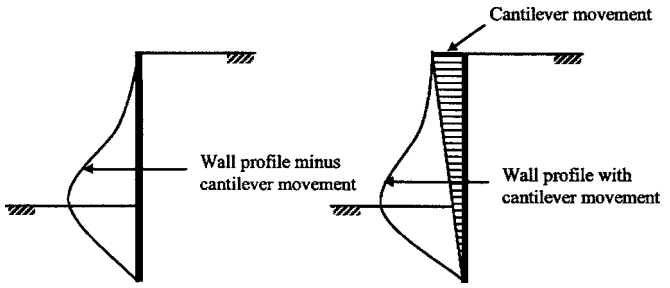

Fig. 5. Effect of cantilever stage movements on system displacement [adapted from Clough et al. (1989)]

roughly equal, the following design method for braced excavations will be based on $c_{u,\mathrm{DSS}}$. The same decision was made by O'Rourke (1993).

Virtual Work

The equilibrium of the unbalanced weight of soil inside the mechanism is provided by the mobilized shear strength $c_{\mathrm{mob}}=\beta c_{u,\mathrm{DSS}}$ which increases as the excavation proceeds in stages. The value of β appropriate to the completion of some stage can be found using the Principle of Virtual Work. The virtual strains and displacements compatible with the current geometry of the mechanism are to be taken as the incremental shear strain $\delta\gamma\approx(2\delta w_m/\ell)$ and the maximum incremental soil displacement δw_m which give rise to vertical settlements δv. Then, the virtual loss of potential energy balances the virtual plastic work in distributed shearing:

$$\int_{\mathrm{vol}} \gamma_t \delta v d\mathrm{vol} = \int_{\mathrm{vol}} c_{\mathrm{mob}} \delta\gamma d\mathrm{vol} \tag{5}$$

where γ_t=unit weight of soil per unit volume so that

$$\beta = \frac{\int \gamma_t \delta v d\mathrm{vol}}{\int c_u \delta\gamma d\mathrm{vol}} \tag{6}$$

Calculation Process

The calculation is carried out as follows.

1. At each stage of the excavation, the proportional strength mobilized ($\beta=c_{\mathrm{mob}}/c_u$) due to the excavation of soil beneath the lowest support is obtained from Eq. (6), performing appropriate integrations that respect the strength profile.
2. The corresponding mobilized shear strain γ_{mob} is found from the stress-strain curve obtained from a DSS test on a representative undisturbed sample, and normalised in terms of β versus γ.
3. The engineering shear strain increment $\delta\gamma$ due to the current stage of excavation is then calculated.
4. The incremental wall movement δw_m is then calculated from Eq. (4).
5. Then, the incremental wall movement profile is plotted using the cosine function of Eq. (1).
6. The cumulative displacement profile is obtained by accumulating the incremental movement profiles.

Cantilever Movement

In an ideal excavation process, the first level of supports is installed at an early stage in order to minimize cantilever movements in the wall. However, this may not be possible in practice due to the variety of site conditions and construction sequences. For example, the use of berms and rakers makes it difficult to install supports unless significant excavation is made. Clough et al. (1989) suggest that the movements due to the cantilever mechanism and the bulging mechanism can be added to obtain the final movement (Fig. 5). Fig. 6 shows the results of finite element (FE) analyses carried out by Hashash (1992) for a braced excavation supported by a 60 m deep wall. The solid lines represent the wall movements retaining a braced excavation that has an initial unsupported height of 5 m. The solid-dashed lines represent the wall movement assuming that the first support is installed at ground level prior to the excavation. The dashed lines with solid square markers represent the predicted total wall movements obtained by adding the bulging movement to the movements of a cantilever wall with 5 m excavation in accordance with Clough et al. (1989). Although the superposed wall movements do not

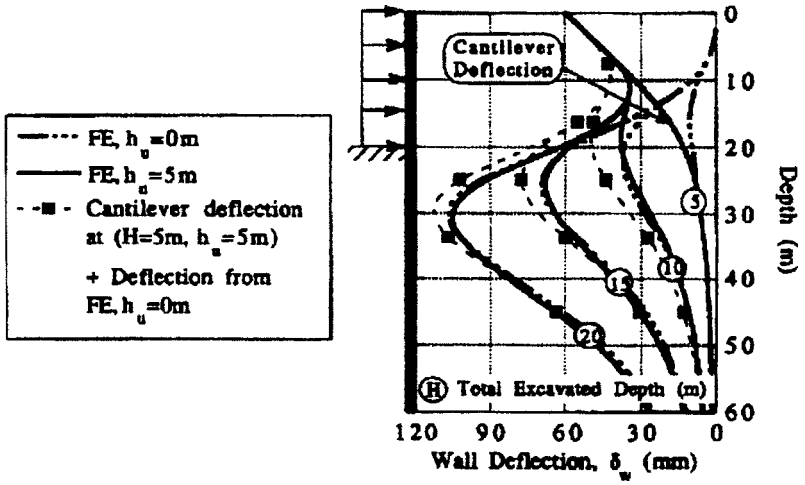

Fig. 6. Comparison between FE analysis and the Clough et al. (1989) method for the effects of cantilever stage movements on system displacement [Hashash (1992); reproduced with permission from MIT]

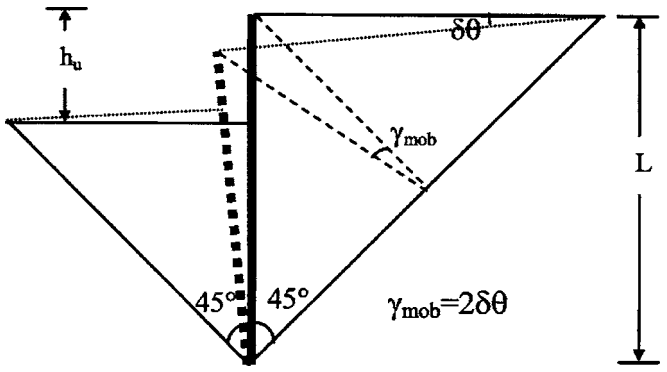

Fig. 7. Plastic deformation mechanism for cantilever retaining walls in undrained conditions

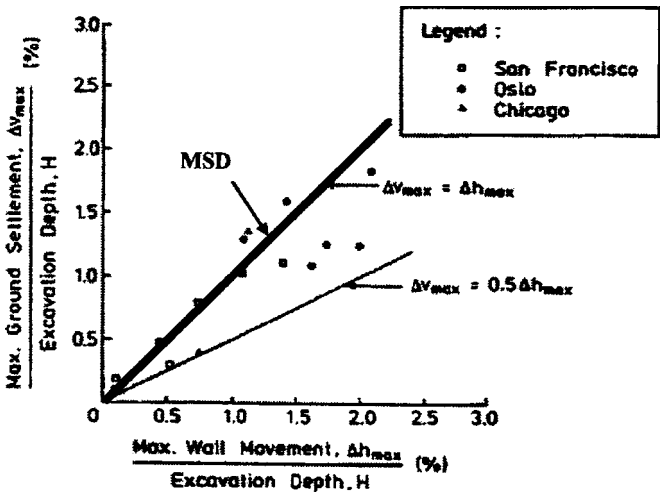

Fig. 8. Relationship between maximum ground settlements and maximum lateral wall movements [adapted from Mana and Clough (1981), ASCE]

match exactly the actual computed movements, the discrepancies in the pattern and the magnitude of the predicted movements are not significant.

Following Bolton and Powrie (1988) and Osman and Bolton (2004), the deformation around a cantilever retaining wall can be idealized by means of triangles, one on each side of the wall, deforming in uniform shear (Fig. 7) such that the mobilized shear strain γ_{mob} is twice the wall rotation $\delta\theta$. The proportional strength mobilized ($\beta=c_{mob}/c_u$) can then be obtained by Virtual Work, using appropriate integrals in Eq. (6). The corresponding mobilized shear strain γ_{mob} is found from the representative stress-strain curve. Then, the angle of wall rotation $\delta\theta$ is obtained by dividing the mobilized shear strain by 2 and the displacement at the top of the wall is calculated by multiplying the angle of wall rotation by the wall length.

Surface Settlement behind the Wall

Mana and Clough (1981) analyzed field data from excavations in soft clay by relating the maximum lateral wall displacements to the maximum surface settlement behind the wall as shown in Fig. 8. It can be seen that settlements range from 0.5 to 1.0 times the lateral wall movements. The plastic deformation mechanism assumed in the mobilizable strength design (MSD) method predicts maximum settlements that are always equal to the maximum wall movements (Fig. 3). From the data shown in Fig. 7, this would appear to be a useful and conservative design expedient.

Finite Element Validation

The validity of the assumptions used in the MSD method is examined by comparing with the results of comprehensive FE analyses of plane strain braced excavations in Boston blue clay carried out by Hashash and Whittle (1996). In these analyses, the MIT-E3 constitutive model is used (Whittle 1987, 1993; Whittle and Kavvadas 1994; Whittle et al. 1994). This model is capable of simulating small strain nonlinearity, soil strength anisotropy, and hysteretic and inelastic behavior associated with reversal in load directions. In the FE analyses, the excavation was assumed to be 40 m wide supported by a 0.9 m thick concrete wall (Fig. 9).

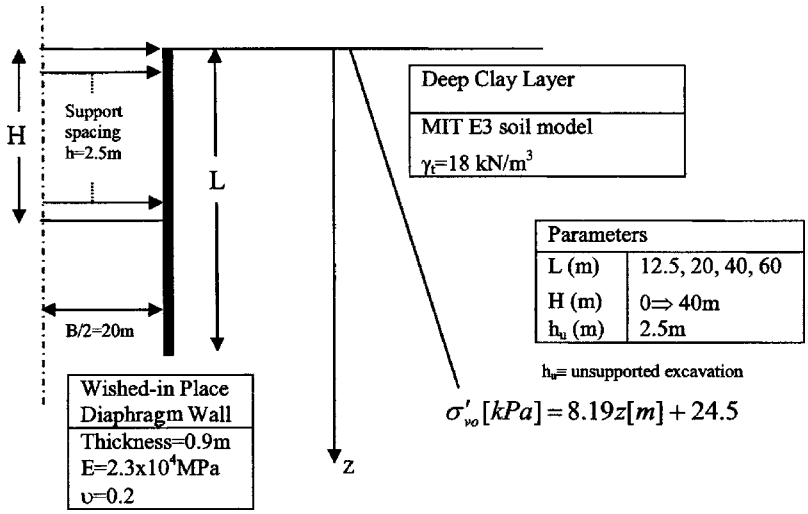

Fig. 9. Initial conditions and geometric parameters [adapted from Hashash and Whittle (1996)]

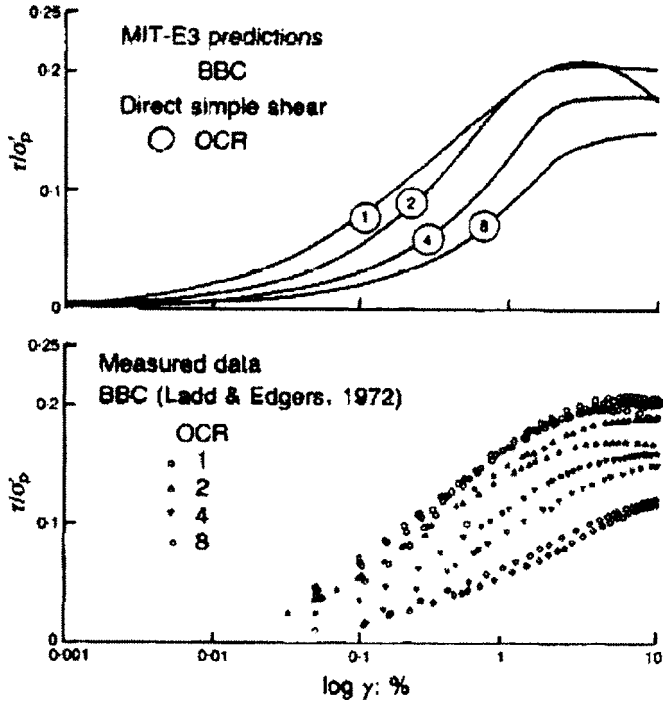

Fig. 10. Stress-strain response for K_o consolidated undrained DSS tests on Boston blue clay [Whittle (1993); reproduced with permission from the Institution of Civil Engineers, London, U.K.]

Soil Behavior in the MSD Method

The soil strength is assumed to be isotropic and the undrained strength is obtained from DSS data. Fig. 10 shows stress-strain relations for Boston blue clay obtained from laboratory tests (Ladd and Edgers 1972) and from FE simulations using the MIT-E3 constitutive model (Whittle 1993). Table 2 shows the ratio of c_u/σ'_{vo} in the DSS mode for different overconsolidation ratios (OCRs). The undrained strength profiles in the MSD calculations are derived using the effective vertical stress profile of Fig. 9 together with c_u/σ'_{vo} ratios predicted by the MIT-E3 model in the simulations of DSS tests (Whittle 1993), and listed in Table 2.

Comparison between FE and MSD

Fig. 11 compares the wall lateral displacements calculated by the MSD method and those obtained using FE analysis for four different wall lengths (L=12.5, 20, 40, and 60) at various stages of excavation in K_o normally consolidated soil (OCR=1) and comparative displacements for 60 m walls for OCRs of 2 and 4. All of the walls are braced at a vertical spacing h=2.5 m, while the first support is installed after excavation to an unsupported depth h_u=2.5 m. The wall end condition is assumed to be free (α=2) for short walls (L=12.5 and L=20) since the clay is very deep and very soft at the base and the embedded length is not long enough to restrain the movement at the tip of the wall. For long walls (L=40 and L=60), the embedded depth was assumed to be sufficient to restrain the movement at the wall base. A constant value of α=4/3 was assumed which gives a point of inflection at the bottom of the wall. An example illustrating the MSD calculations is given in the Appendix.

Table 2. Ratio of Undrained Shear Strength to the Effective Vertical Stress (c_u/σ'_{vo})in the DSS of Shearing Mode for Different OCR

	c_u/σ'_{vo}			
Measurements	OCR=1.0	OCR=2.0	OCR=4.0	OCR=8.0
Laboratory (Ladd and Edgers 1972)	0.21	0.34	0.60	0.96
FE MIT-E3 (Whittle 1993)	0.21	0.41	0.77	1.19

The results show that there is a general similarity in the deformation trends. However, the MSD method appears to overestimate the initial cantilever wall movements, which correspond more to base sliding whereas the MSD assumes rotation about the base. The discrepancies in deformation profiles for long walls (L=40, L=60) appear to be due to the simplification in modeling the wall end condition (α=4/3) and the use of the empirical cosine function [Eq. (1)]. For the more significant movements of longest walls subject to the deepest excavations, the MSD calculations ranged from an overprediction by a factor of 1.15 to an underprediction by factor 0.6.

Field Validation

The usefulness of the MSD method in practical applications is demonstrated for published case histories of braced excavations in Boston, San Francisco, and Oslo.

Post Office Square Garage, Boston

Post Office Square Garage was constructed with seven levels of below-grade structure in the heart of the downtown financial district of Boston in late 1980s. Details of construction and performance were documented by Becker and Haley (1990), Whitman et al. (1991), and Whittle et al. (1993). The structure consists of a cast-in-place 0.9 m concrete diaphragm wall around the garage perimeter, extended down into the bedrock and braced internally by the floor slabs.

Subsurface soils at the site (Fig. 12) comprise 0.6 to 4.0 m fill, 10 to 15 m thick clay (Boston blue clay), 0.3 to 5.8 m sand, 1.5 to 11.6 m till, and bedrock. The actual soil profile is therefore complex and variable. The DSS undrained strength profile for the clay adopted in the calculations is shown in Fig. 12. This profile is generated from the average OCR profile assumed by Whittle et al. (1993) and the normalized value of c_u/σ'_{vo} obtained from undrained DSS tests on Boston blue clay (Ladd and Edgers 1972) as given in Table 2. A conservative approach is followed by assuming that the stiffness of the till and the sand is the same as that of the clay at the corresponding depth. The intention is that the MSD method should be based on the average soil properties in the zone of plastic deformation. Since the clay has an OCR varying from 6 to 2, the normalized stress-strain curve for OCR=4 is taken as representative (Fig. 10).

Fig. 13 presents measurements of lateral deflections from two inclinometers on the perimeter of the site compared with the MSD predictions. The different trends observed, and predicted, for Milk Street and Pearl Street are due to differences in the construction sequence. Near Milk Street (Fig. 13), the roof slab was constructed prior to the excavation; whereas at other locations, the excavation was initially unsupported to a maximum depth up to 6 m. Two MSD calculations were carried out assum-

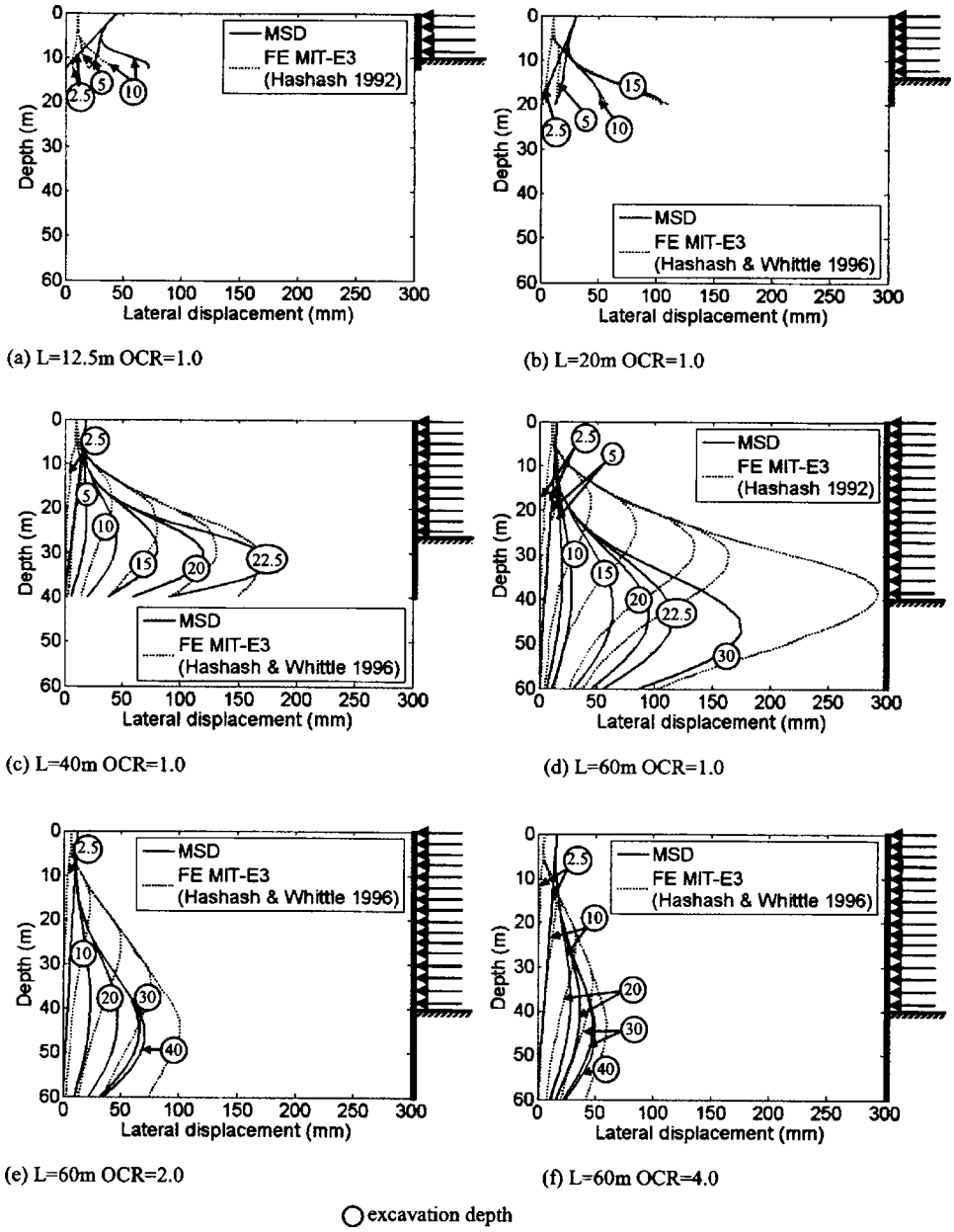

Fig. 11. Comparison between MSD and FE for lateral displacement profiles: (a) $L=12.5$, OCR=1.0; (b) $L=20$ m, OCR=1.0; (c) $L=40$ m, OCR=1.0; (d) $L=60$ m, OCR=1.0; (e) $L=60$ m, OCR=2.0; and (f) $L=60$ m OCR=4.0

ing 0 and 6 m of unsupported excavation. In the MSD, the supports are assumed rigid; no shrinkage is allowed to occur at the roof slab. This may explain the small underpredictions (circa 8 mm) in the crest displacements. However, MSD estimations for the maximum movements at the end of excavation are generally in good agreement with the measured data (±5 mm).

The wide scatter in the field settlement measurements (Fig. 14) is likely to be due to the variation of construction sequences and soil strata. The localization of settlement adjacent to the excavation is predicted successfully by the MSD method. The figure shows also that the maximum settlement predicted by the MSD method (circa 47 mm) conforms well to the maximum observed field measurements. The settlement trough predicted by the MSD method extends to 25 m from the wall. Although this certainly covers the zone of most significant settlement, measurements of about 3 mm were still recorded at 40 m. The FE analysis carried out by Whittle et al. (1993) appears to overpredict the extension of the settlement trough and to underpredict the maximum settlement.

Davidson Avenue, San Francisco

During 1977–1978, a series of large sewer culverts was constructed in the Islais Creek Basin near San Francisco Bay. The culverts are about 8 m wide and 9 m deep. Sheet-pile walls of 13 m depth were used to support the excavations for the culverts. The wall was braced by four levels of struts with a vertical spacing of 1.8 to 4.3 m. Details of construction sequences and performance were documented by Clough and Reed (1984). The uppermost soil in the Islais Creek is Young Bay mud consisting of soft clay of 12 to 18 m thickness. DSS test data reported by Hunt et al. (2002) are shown normalized in Fig. 15. Fig. 16 gives

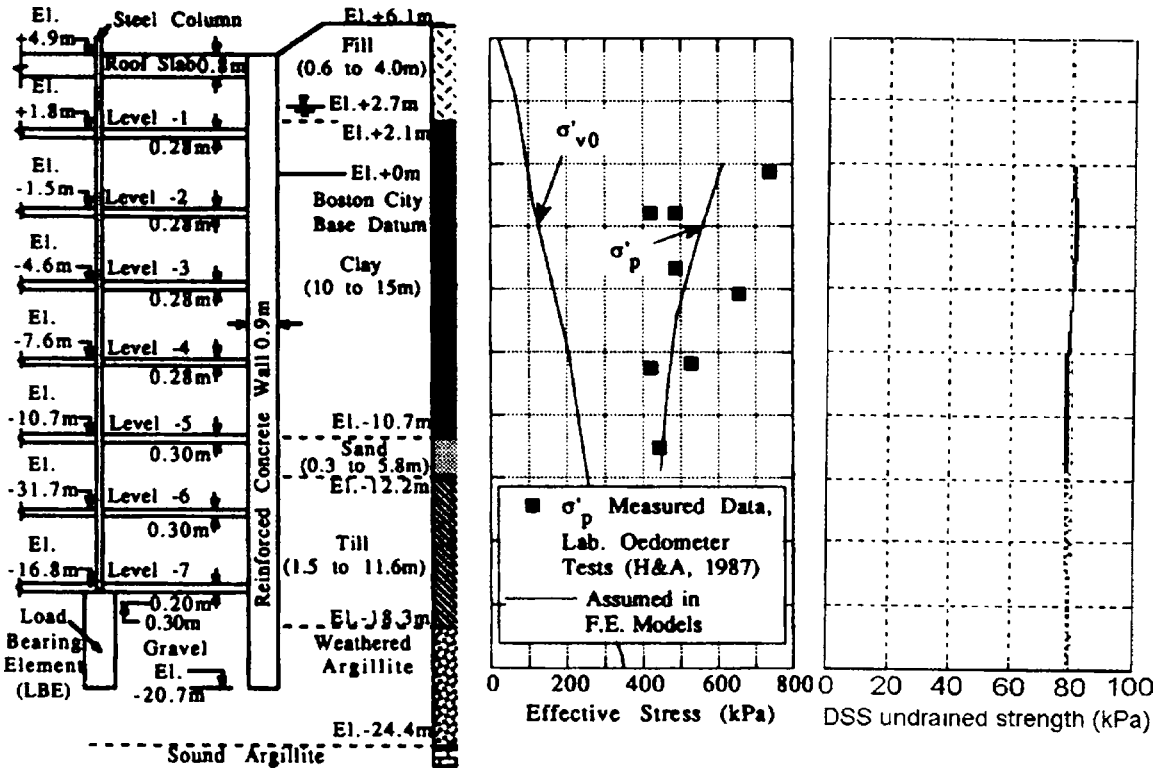

Fig. 12. Post Office Square Garage structure and initial soil conditions [adapted from Whittle et al. (1993)]

a cross section at Davidson Avenue and shows that the lateral wall movements are predicted well by the MSD method (circa 20% overprediction).

Vaterland 1, Oslo

Vaterland 1 is one of several test sections on the Oslo Subway System. It was instrumented and documented by Norwegian Geotechnical Institute (1962). The excavation was 11 m wide and 8 m deep, on average. The excavation was supported by a sheet pile wall of depth 14 m. The wall is braced by five levels of struts with a vertical spacing varying between 1.2 and 2 m. The site is underlain by up to 16 m of soft clay over bedrock. A layer of fill above the clay was taken to apply a surcharge pressure of 39 kPa on the retained clay, which has a unit weight $\gamma_t = 19.5$ kN m^3.

An MSD backanalysis was carried out using the stress-strain data obtained from direct simple shear tests by Bjerrum and Landva (1966) and shown in Fig. 17. A cross section at Vaterland 1 (Zone 4) is given in Fig. 18, together with a comparison of MSD predictions against field measurements. The MSD method overestimates lateral displacements in the early excavation stages by about 50%, possibly due to inaccurate small-strain measurements, but its predictions in the middle stages become more accurate. Finally, MSD predicts a maximum cumulative wall movement of 180 mm at an excavation depth of 8 m just before the last props are inserted, and predicts instability just before an excavation depth of 9 m with the demanded strength having exceeded the peak strength available in Fig. 17 due to the soil shear strain having exceeded 6.5%. The field measurements of

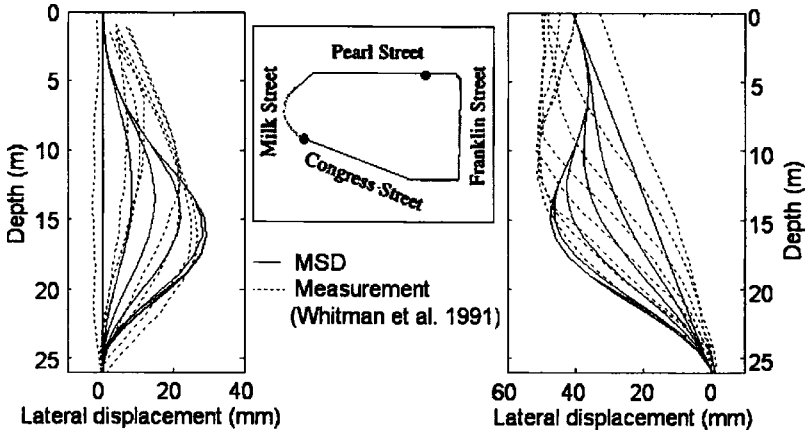

Fig. 13. Predicted and measured lateral displacements at Post Office Square Garage

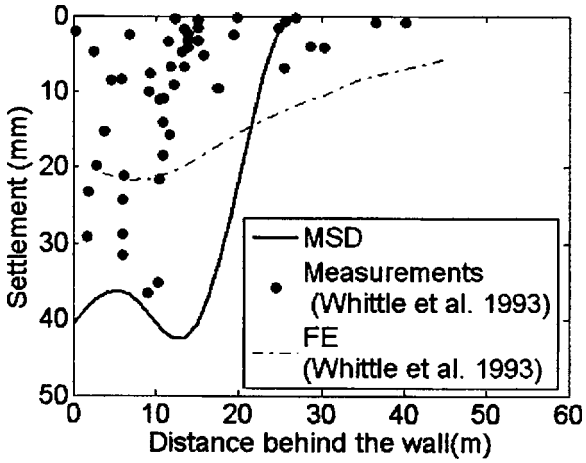

Fig. 14. Comparison of predicted and measured surface settlements after the installation of the sixth floor at Boston Post Office Square Garage

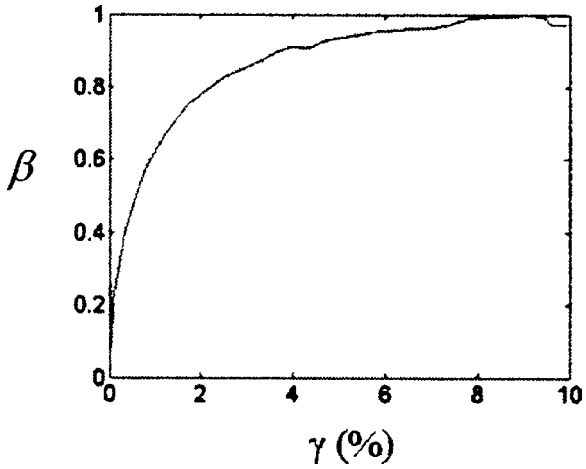

Fig. 15. Normalized stress-strain response from a K_o-consolidated undrained DSS test on Young Bay mud at Islais Creek [data adapted from Hunt et al. (2002)]

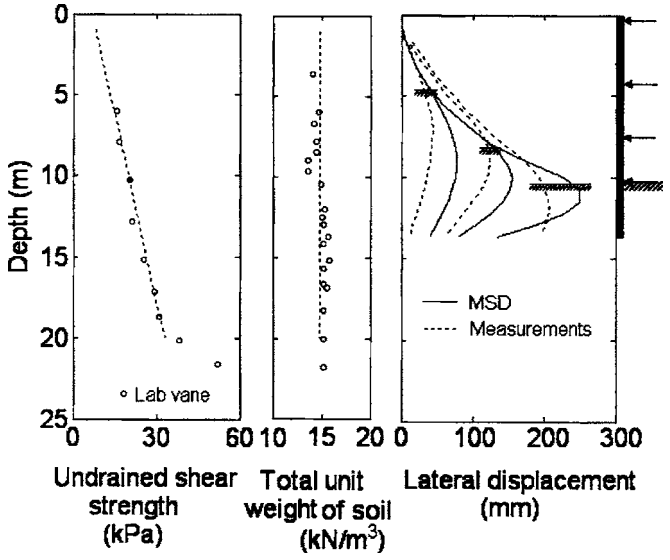

Fig. 16. Davidson Avenue: Soil properties and lateral displacements [measurements from Clough and Reed (1984)]

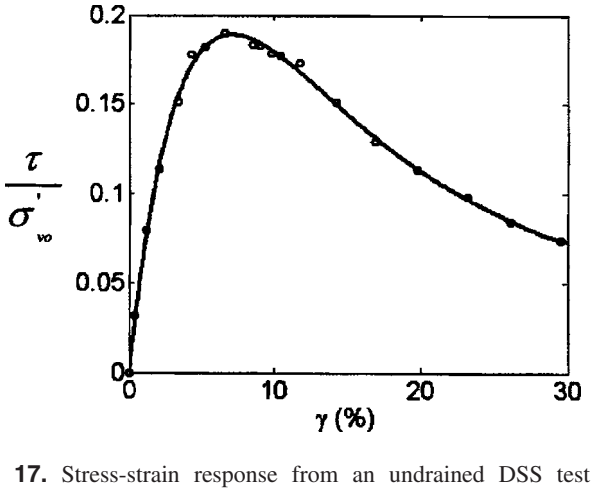

Fig. 17. Stress-strain response from an undrained DSS test on Norwegian quick clay [Bjerrum and Landva (1966); reproduced with permission from the Institution of Civil Engineers, London, U.K.]

maximum wall movement gave 158 mm at 6.2 m excavation depth and 223 mm at 9 m, showing that MSD has again erred slightly on the conservative side. This tendency is thought to be due to omitting from the current MSD analysis the work done in flexing the wall; O'Rourke (1993) showed that an allowance for wall bending resistance was successful in explaining the delayed instability in the Oslo field trials. Although such an allowance would be easy to incorporate, the real lesson of this example is that MSD would assist an engineer in assuring that such large deformations do not occur.

Conclusions

A new class of plastic deformation mechanism for displacement calculations of braced excavations has been developed. In these mechanisms, the soil is assumed to shear and deform compatibly and continuously with no relative sliding at the boundaries. These mechanisms take into account the variation of the shear strength

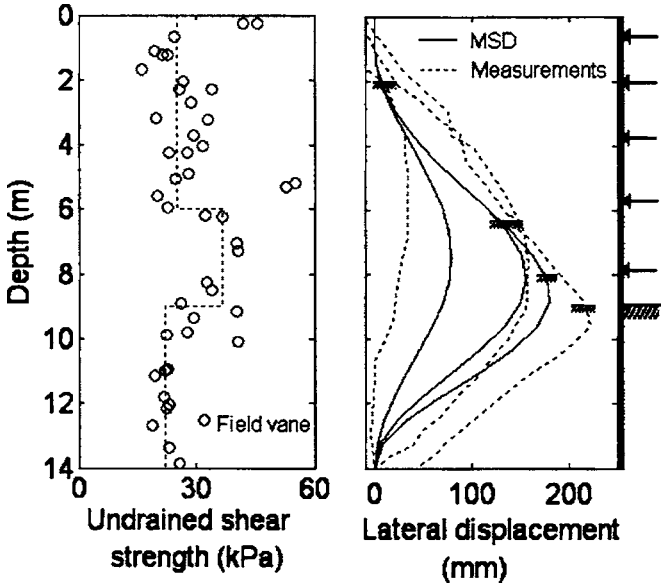

Fig. 18. Cross section at Vaterland 1, Oslo

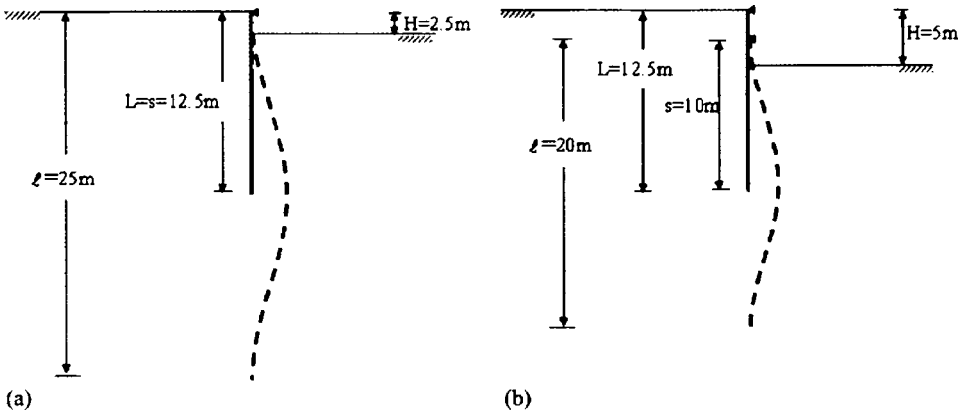

Fig. 19. Bulging incremental movement: (a) Step 2 and (b) Step 3

with depth, the flexibility of the wall, and the vertical spacing of the bracing. The key advantage is that the shear strength mobilized in the soil around excavations can be directly related to the ground displacements.

Modeling soil stiffness properly in the analysis and design of braced excavations is very important. The selection of a characteristic stress-strain curve is obviously necessary in design, but is difficult to decide. The designer should select a stress-strain curve appropriate to the average soil behavior in the zone of plastic deformation taking anisotropy into account. The writers show that the undrained DSS test gives good displacement predictions. Since triaxial tests are more commonly available in practice, further investigation of the appropriate stiffness anisotropy factors at moderate strains, perhaps modifying the strength anisotropy factors of Clough and Hansen (1981), would be beneficial.

The MSD predictions in this paper give errors rather smaller than a factor of 2. The nonlinear sequential displacement of braced excavations has been shown in three studies of field cases to be predicted sufficiently accurately (within about 20%), and rather simply by the MSD method in the range of greatest practical interest (50 to 100 mm).

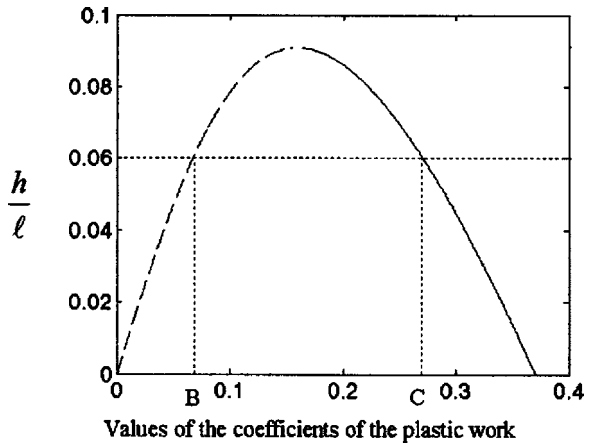

Fig. 20. Values of coefficients of the plastic work in the distributed shearing zone EFH (coefficients *B* and *C* of Table 3)

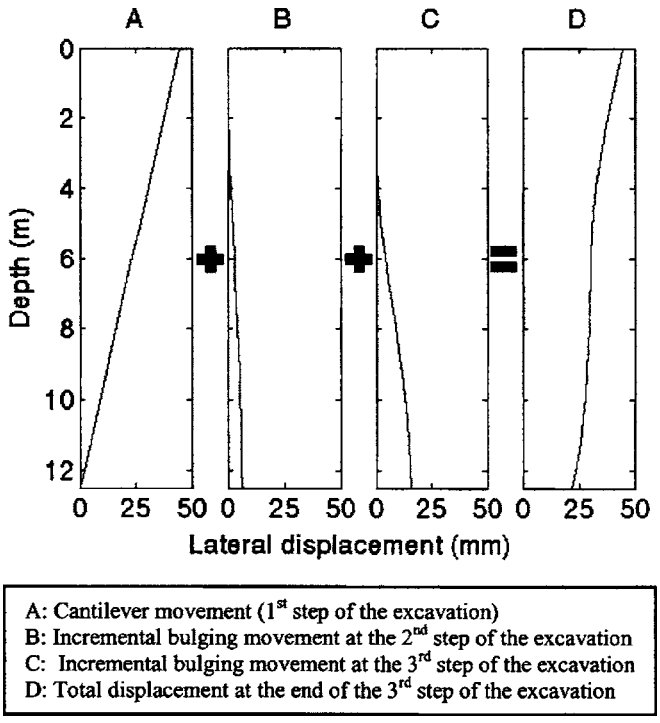

Fig. 21. Calculation example (L=12.5 m, H=5 m, h_u=2.5, h=2.5 m, and OCR=1.0)

Acknowledgments

The writers are grateful to Cambridge Commonwealth Trust and to the Committee of Vice-Chancellors and Principals of U.K. universities (Overseas Research Scheme) for their provision of financial support to the first writer.

Appendix. Calculation Example

The following example shows the MSD calculation of wall deflection for a 12.5 m wall retaining a 5 m excavation [Fig. 11(a)]. The construction sequence is comprised of the following steps: (1) The soil is excavated initially to an unsupported depth h_u of 2.5 m; (2) the first support is installed at the ground surface; (3) a second level of supports is installed at a vertical spacing of 2.5 m and 2.5 m of the soil is excavated. The undrained strength is given by: $c_u=c_o+c_1z=0.21$ [$8.19z+24.5$] kPa, where c_o=undrained shear strength at the ground surface, c_1=rate of variation of undrained shear strength with depth, and z=depth below ground surface.

Table 3. Virtual Work Calculations in Plastic Deformation Mechanisms for Braced Excavations

Zone	Virtual plastic work in distributed shearing	Virtual loss of potential energy
ABDC	$\beta\delta w_m[2(H-h)c_0+(H-h)^2c_1]$	$\gamma_t\frac{\delta w_m \ell}{2}(H-h)$
CDE	$\beta\frac{\delta w_m \ell}{4\pi^2}\begin{bmatrix}2\pi^2(\pi+\sin(2A\pi)-2A\pi\cos^2(A\pi))(c_0+c_1H)\\+4A\pi^3 h\cos^2(A\pi)c_1+(-6\ell+3\pi^2\ell-2\pi^3 h\\+6\ell\cos^2(A\pi))c_1-2A^2\pi^2\ell(\cos^2(A\pi)-1)c_1\\+2\pi(3A\ell-\pi h)\sin(2A\pi)c_1\end{bmatrix}$	$\frac{1}{4}\delta w_m\gamma_t\ell^2$
EFH	For $\frac{h}{\ell}>0.0908$:	
	$\beta\frac{\delta w_m \ell}{8\pi^2}\begin{bmatrix}2\pi^3\left(1-\frac{h}{\ell}\right)(c_0+c_1H)+\pi^2\sin\left(\frac{2\pi h}{\ell}\right)(c_0+c_1H)\\+3\sqrt{2}\pi^2\ell\left(1-\frac{h}{\ell}\right)^2c_1-\frac{3\sqrt{2}}{2}\ell\left(1-\cos\left(\frac{2\pi h}{\ell}\right)\right)c_1\end{bmatrix}$	$-\gamma_t\delta w_m\ell^2\frac{2-\sqrt{2}}{8\pi^2}\begin{bmatrix}\left(3-2\cos^2\left(\frac{\pi h}{\ell}\right)\right)\cos^2\left(\frac{\pi h}{\ell}\right)\\-\frac{1}{2}\sin^2\left(\frac{2\pi h}{\ell}\right)\\+\pi^2\left(1-\frac{h}{\ell}\right)^2-1\end{bmatrix}$
	For $\frac{h}{\ell}<0.0908$:	
	$\beta\frac{\delta w_m \ell}{8\pi^2}\begin{bmatrix}4\pi^3(B\cos^2(B\pi)-C\cos^2(C\pi))(c_0+c_1H)\\-2\pi^2(\sin(2B\pi)-\sin(2C\pi))(c_0+c_1H)\\+2\pi^3\cos^2\left(\frac{\pi h}{\ell}\right)\left(1-\frac{h}{\ell}\right)(c_0+c_1H)\\+\pi^2\sin\left(\frac{2\pi h}{\ell}\right)(c_0+c_1H)+\sqrt{2}\pi^2\left(1-\frac{h}{\ell}\right)^2\left(4\cos^2\left(\frac{\pi h}{\ell}\right)-1\right)\ell c_1\\+3\sqrt{2}\pi\sin\left(\frac{2\pi h}{\ell}\right)\left(1-\frac{h}{\ell}\right)\ell c_1-2\sqrt{2}\pi^2(B^2-C^2)\ell c_1\\-6\sqrt{2}\pi(B\sin(2B\pi)-C\sin(2C\pi))\ell c_1\\+8\sqrt{2}\pi^2(B^2\cos^2(B\pi)-C^2\cos^2(C\pi))\ell c_1\\+6\sqrt{2}(\sin^2(B\pi)-\sin^2(C\pi))\ell c_1+3\sqrt{2}\sin^2\left(\frac{\pi h}{\ell}\right)\ell c_1\end{bmatrix}$	
FIH	$\beta\frac{\delta w_m}{16}\begin{bmatrix}8(2\ell-3h)(c_0+c_1H)-4\frac{\ell}{\pi}\sin\left(\frac{2\pi h}{\ell}\right)(c_0+c_1H)\\+\sqrt{2}\frac{\ell^2}{\pi^2}\left(3\pi^2-2-2\cos^2\left(\frac{\pi h}{\ell}\right)\right)c_1-2\sqrt{2}h(4\ell-3h)c_1\end{bmatrix}$	$-\frac{\sqrt{2}}{8}\delta w_m\gamma_t\begin{bmatrix}(\ell-h)^2\\-\frac{\ell^2}{\pi^2}\sin^2\left(\frac{\pi h}{\ell}\right)\end{bmatrix}$

Note: A, B, and C=proportional factors. $A=0.3701$; B and C are read from Fig. 20 for each h/ℓ (illustration for $h/\ell=0.06$ is shown in the figure).

Cantilever Movement

For the unsupported excavation $h_u=2.5$ m, the mobilization strength ratio β can be calculated from Eq. (6):

$$\beta = \frac{\int \gamma_t v d\text{vol}}{\int c_u \delta\gamma d\text{vol}} = \frac{\frac{\gamma_t}{6}\left[L^2 - \frac{(L-h_u)^3}{L}\right]}{c_0\left[L + \frac{(L-h_u)^2}{L}\right] + c_1\left[\frac{2}{3}L^2 - h_u^2 + \frac{2}{3}\frac{h_u^3}{L}\right]}$$

Thus, $\beta=0.83$. From Fig. 10, the corresponding mobilized strain γ_{mob} is 0.71%. Therefore, the wall rotation $\delta\theta=\gamma_{mob}/2=0.36\%$ and the crest displacement is $\Delta=\delta\theta^* L = 0.36/100\times 12.5\times 1{,}000=44$ mm.

Bulging Movement

The first support is then installed at the top of the wall [Fig. 19(a)]. The length of the wall below the support $s=L=12.5$ m, and the wavelength $\ell=\alpha s=2\times 12.5=25$ m. Table 3 together with Fig. 20 give expressions for the virtual loss of potential energy and the virtual plastic work in distributed shearing for each zone of the proposed deformation mechanism of Fig. 3. The value of β must then be calculated from Eq. (6). In the particular case of the ground having a linear undrained strength profile, the elements of the integration required in Eq. (6) are detailed in Table 3. Both the virtual plastic work and the virtual loss of potential energy are listed for each of the four zones of shearing set out in Fig. 3. The integration of plastic work involves the *magnitude* of shear strain increments, and therefore requires care when the algebraic value listed in Table 1 goes negative. This leads to the alternative expressions for the plastic work in zone EFH for different ratios of excavation increment h to the wavelength ℓ as listed in Table 3. The coefficients B and C are obtained from the roots of the algebraic expression in Table 1, and plotted for convenience in Fig. 20. Taking $h/\ell=2.5/25=0.1$, the condition $h/\ell>0.0908$ in Table 3 is satisfied, and the outcome of the integration gives:

$$\beta = \frac{\int \gamma_t v d\text{vol}}{\int c_u \delta\gamma d\text{vol}} = 0.27$$

From the MIT-E3 simulated stress-curve for OCR=1, Fig. 10, the corresponding mobilized strain is $\gamma_{mob}=0.05\%$. The maximum incremental wall movement is calculated from Eq. (7):

$$\delta w_m = \frac{\delta\gamma\ell}{2} = \frac{0.05\times 25}{2}\times\frac{1{,}000}{100} = 6 \text{ mm}$$

Similarly, for the third step of excavation [Fig. 19(b)]: $H=5$ m, $h=2.5$ m, $s=L-h=10$ m, and the wavelength $\ell=\alpha s=2\times 10=20$ m. The mobilization ratio $\beta=0.53$ and the corresponding shear strain is $\gamma_{mob}=0.21\%$. Thus, the shear strain increment in this step of excavation is $0.21\%-0.05\%=0.16\%$. Therefore, the maximum incremental displacement is 16 mm.

Finally, the incremental bulging movement profile in each stage is plotted using the cosine function [Eq. (1)], the maximum incremental displacement in each stage, and the corresponding wavelength. The total wall deflection is then obtained by adding the cantilever movement and the total bulging movement (Fig. 21).

References

Becker, J. M., and Haley, M. X. (1990). "Up/down construction—Decision making and performance." *Proc., ASCE Conf. the Design and Performance of Earth Retaining Structures, Geotech. Spec. Publ. No. 25*, ASCE, New York, 170–189.

Bjerrum, L., and Landva, A. (1966). "Direct simple-shear test on a Norwegian quick clay." *Geotechnique*, 16(1), 1–22.

Bjerrum, L., and Eide, O. (1956). "Stability of strutted excavations in clay." *Geotechnique*, 6(1), 115–128.

Bolton, M. D., and Powrie, W. (1988). "Behavior of diaphram walls in clay prior to collapse." *Geotechnique*, 38(2), 167–189.

Clough, G. W., and Hansen, L. A. (1981). "Clay anisotropy and braced wall behavior." *J. Geotech. Eng. Div., Am. Soc. Civ. Eng.*, 107(7), 893–913.

Clough, G. W., Smith, E. M., and Sweeney, B. P. (1989). "Movement control of excavation support systems by iterative design." *Proc., ASCE Found. Engrg. Congr.*, ASCE, New York, Vol. 1, 869–884.

Clough, G. W., and Reed, M. W. (1984). "Measured behavior of braced wall in very soft clay." *J. Geotech. Eng.*, 110(1), 1–19.

Eide, O., Aas, G., and Josang, T. (1972). "Special application of cast-inplace walls for tunnels in soft clay." *Proc., 5th European Conf. on Soil Mechanics and Foundation Engineering*, Madrid, Spain, 1, 485–498.

Garrett, C., and Barnes, S. J. (1984). "Design and performance of the Dunton Green retaining wall." *Geotechnique*, 34(4), 533–548.

Hashash, Y. M. A., and Whittle, A. J. (1996). "Ground movement prediction for deep excavations in soft clay." *J. Geotech. Eng.*, 122(6), 474–486.

Hashash, Y. M. A. (1992). "Analysis of deep excavations in clay." Ph.D. thesis, MIT, Cambridge, Mass.

Hunt, C. E., Pestana, J. M., Bray, J. D., and Riemer, M. (2002). "Effect of pile driving on static and dynamic properties of soft clay." *J. Geotech. Geoenviron. Eng.*, 128(1), 13–24.

Ikuta, Y., Maruoka, M., Aoki, M., and Sato, E. (1994). "Application of the observational method to a deep basement excavated using the top-down observation method." *Geotechnique*, 44(4), 655–664.

Ladd, C. C., and Edgers, L. (1972). "Consolidated-undranined direct simple shear tests on Boston blue clay." *Res. Report R72-82*, MIT, Cambridge, Mass.

Lambe, T. W. (1967). "Stress path method." *J. Soil Mech. Found. Div.*, 93(6), 309–331.

Mana, A. I., and Clough, G. W. (1981). "Prediction of movements for braced cuts in clay." *J. Geotech. Eng. Div., Am. Soc. Civ. Eng.*, 107(6), 759–777.

Norwegian Geotechnical Institute. (1962). "Measurements at a strutted excavation, Oslo Subway, Vaterland 1." *Tech. Rep. No. 6*, Norwegian Geotechnical Institute, Blindern, Norway.

O'Rourke, T. D. (1993). "Base stability and ground movement prediction for excavations in soft clay." *Retaining structures*, Thomas Telford, London, 131–139.

Osman, A. S., and Bolton, M. D. (2004). "A new design method for retaining walls in clay." *Can. Geotech. J.*, 41(3), 453–469.

Ou, C. Y., Liao, J. T., and Cheng, W. L. (2000). "Building response and ground movements induced by a deep excavation." *Geotechnique*, 50(3), 209–220.

Raison, C. A. (1985). "Discussion on performance of proposed and cantilevered rigid walls." *Geotechnique*, 35(4), 540–544.

Tanaka, H.. (1994). "Behaviour of a braced excavation in soft clay and the undrained shear strength for passive earth pressure." *Soils Found.*, 34(1), 53–64.

Terzaghi, K. (1943). *Theoretical soil mechanics*, Wiley, New York.

Whitman, R. V., Johnson, E. G., Abbott, E. L., and Becker, J. M. (1991). "Field instrumentation plays vital role in deep excavation project." *Proc., Geotech. Engrg. Congress*, Geotech. Spec. Publ. No. 27, ASCE, New York, 1, 173–184.

Whittle, A. J. (1993). "Evaluation of a constitutive model for overconsolidated clays." *Geotechnique*, 43(2), 289–313.

Whittle, A. J. (1987). "A constitutive model for overconsolidated clays with application to the cyclic loading of friction piles." Ph.D. thesis, Dept. of Civil and Environmental Engineering, MIT, Cambridge, Mass.

Whittle, A. J., and Kavvadas, M. (1994). "Formulation of the MIT-E3 constitutive model for overconsolidated clays." *J. Geotech. Eng.*, 120(1), 173–198.

Whittle, A. J., DeGroot, D. J., Ladd, C. C., and Seah, T. H. (1994). "Model prediction of anisotropic behavior of Boston blue clay." *J. Geotech. Eng.*, 120(1), 199–224.

Whittle, A. J., Hashash, Y. M. A., and Whitman, R. V. (1993). "Analysis of deep excavation in Boston." *J. Geotech. Eng.*, 119(1), 69–90.

Young, D. K., and Ho, E. W. L. (1994). "Observational approach to design of a sheet-piled retaining wall." *Geotechnique*, 44(4), 637–654.